European Journal of Mechanics A/Solids 65 (2017) 243–256

Contents lists available at ScienceDirect

European Journal of Mechanics A/Solids

journal homepage: www.elsevier.com/locate/ejmsol

Electromechanical macroscopic instabilities in soft dielectric elastomer composites with periodic microstructures

Artemii Goshkoderia, Stephan Rudykh*

Department of Aerospace Engineering, Technion – Israel Institute of Technology, Haifa 32000, Israel

ARTICLE INFO

Article history:
Received 26 December 2016
Received in revised form
14 April 2017
Accepted 25 April 2017
Available online 4 May 2017

Keywords:
Dielectric elastomers
Stability
Composites
Finite deformation
Macroscopic instabilities
Microstructure

ABSTRACT

We study electromechanical macroscopic instabilities in dielectric elastomer (DE) composites undergoing finite strains in the presence of an electric field. We identify the unstable domains for DE composites with periodically distributed circular and elliptical inclusions embedded in a soft matrix. We analyze the influence of the applied electric field and finite strains, as well as the microstructure geometrical parameters and material properties, on the stability of the DE composites. We find that the unstable domains can be significantly tuned by an electric field, depending on the electric field direction relative to pre-stretch and microstructure. More specifically, the electric field aligned with the stretch direction, promotes instabilities in the composites, and the electric field applied perpendicularly to the stretch direction, stabilizes the composites. Critical stretch decreases with an increase in the volume fraction of circular inclusions. An increase in the contrast between the dielectric properties of the constituents, magnifies the role of the electric field, while an increase in the shear modulus contrast results in a less stable DE composite. For periodic DE composites with elliptical inclusions, we find that the critical stretch depends on the inclination angle of the inclusion, and that the critical stretch reaches a unique maximum at an angle defined by the inclusion ellipticity aspect ratio. In the aligned case – when the longest side of the inclusion is aligned with the stretch direction – an increase in the ellipticity ratio results in an increase in critical stretch.

1. Introduction

Dielectric elastomers (DEs) can achieve large deformations when excited by an electric field (Pelrine et al., 1998, 2000b, 2000a). This ability, together with their lightweight, fast response time and flexibility, make DEs attractive for a wide and diverse variety of applications, such as artificial muscles (Bar-Cohen, 2001), energy-harvesting and noise canceling devices, soft robotics (Kornbluh et al., 2012; McKay et al., 2010; Carpi et al., 2011; Bortot et al., 2016), and tunable waveguides (Gei et al., 2011; Galich and Rudykh, 2016). However, the wide spread usage of DEs has been limited due to the extremely high electric fields required to achieve large strains. Thus, DEs need to operate at the risky edge of electromechanical instabilities (Plante and Dubowsky, 2006; Rudykh et al., 2012; Keplinger et al., 2012; Li et al., 2013). A promising approach for reducing the required electric field is to design and fabricate composite materials with an enhanced electromechanical coupling. Experimental studies show significant enhancements in the electromechanical coupling in DE composites (Stoyanov et al., 2011; Huang and Zhang, 2004). Moreover, theoretical estimates and numerical simulations (Tian et al., 2012; Rudykh et al., 2013) predict even more significant improvements in the performance of DE composites with periodic microstructures. Thus, improvement by orders of magnitude in the electromechanical coupling can be achieved in hierarchically structured composites comprising softer and stiffer phases (Rudykh et al., 2013). Recent advances in the microstructured material fabrication and 3D printing, allowing realization of highly structured materials at different length-scales (Kolle et al., 2013; Lee and Fang, 2012; Zheng et al., 2014; Slesarenko and Rudykh, 2016), provide a great perspective for this approach for enhancing DE performance.

The foundation for the non-linear electroelasticity theory was laid by the pioneering works by Toupin (1956, 1960) showing that electromechanical coupling in DEs is characterized by a quadratic dependence on the applied electric field. Recently, the electroelasticity theory of finite deformations has been reformulated by Dorfmann and Ogden (2005, 2010), McMeeking and

* Corresponding author.
E-mail address: rudykh@technion.ac.il (S. Rudykh).

http://dx.doi.org/10.1016/j.euromechsol.2017.04.008
0997-7538/

Landis (2005), and Suo et al. (2008); Zhao and Suo (2010), and, more recently, by Liu (2013), and by Li et al. (2016). Itskov and Khiêm (2014) and Ortigosa and Gil (2016) considered the aspects of the convexity of the electro-elastic energy functions. Cohen et al. (2016), Cohen and deBotton (2016) conducted a statistical-mechanics-based analysis of the response of polymer chain networks in DEs. In parallel, significant efforts have been made towards the development and implementation of the nonlinear electroelasticity framework into numerical schemes (Vu and Steinmann, 2007; Volokh, 2012; Javili et al., 2013; Keip et al., 2014; Galipeau et al., 2014; Jabareen, 2015; Aboudi, 2015). The electromechanical instabilities in finitely deformed homogenous DEs have been analyzed by Zhao and Suo (2007), and Dorfmann and Ogden (2010, 2014), in parallel with the experimental observations of the failure modes such as pull-in instabilities (Plante and Dubowsky, 2006), creasing and surface patterning (Wang et al., 2011). Based on an exact analytical solution available for finitely deformed periodic layered DE composites, the studies of the electromechanical instabilities in the periodic DE laminates have been performed (Bertoldi and Gei, 2011; Rudykh and deBotton, 2011; Rudykh and Bertoldi, 2013; Rudykh et al., 2014). These works show the significant dependence of DE material stability on the applied electric field and pre-stretch. However, the set of microstructures for which exact analytical solutions can be derived is limited; as a result, very little is known about the instabilities in DE composites with particulate and periodic microstructures, which showed promising results of significant enhancement in electromechanical coupling and actuation (Rudykh et al., 2013). Moreover, the knowledge about the instabilities in these microstructured electro-active composites may provide the tools for designing materials with switchable functionalities (Bertoldi et al., 2008; Bertoldi and Boyce, 2008; Krishnan and Johnson, 2009; Rudykh and Boyce, 2014; Singamaneni et al., 2008; 2009).

In this study, we perform an analysis of electromechanical instabilities in finitely deformed DE composites with periodically arranged active particles embedded in a matrix. In particular, we focus on the *macroscopic* stability of periodic two-dimensional DE composites with circular and elliptical inclusions. We implement the electromechanical instability analysis into a numerical finite element based tool, and identify the unstable domains for finitely deformed DE composites in the presence of an electric field. We analyze the influence of the electric field, pre-stretch, microstructure and material parameters on DE composite stability.

The work is structured as follows: Sec. 2 presents the theoretical background for the finitely deformed dielectric elastomers and electromechanical instability analysis previously developed by Dorfmann and Ogden (2005, 2010) and its specification for a plane problem reported in Rudykh et al. (2014). The numerical simulations, including the electromechanical periodic boundary conditions, and the procedure for determination of the electroelastic moduli are described in Sec. 3. In Sec. 4, we apply the stability analysis to identify the unstable domains for the DE composites with periodically distributed circular (4.1) and elliptical (4.2) inclusions embedded in a matrix. Sec. 5 concludes the paper with a summary and a discussion.

2. Theoretical background

We denote by $\mathscr{B}_0$ and $\mathscr{B}$ the regions occupied by a body in the reference and current configurations, respectively. The Cartesian position vector of a material point in the reference configuration of a body is $\mathbf{X}$ and its position vector in the deformed configuration is $\mathbf{x}$. We introduce a mapping vector function $\boldsymbol{\chi}$ such that

$$\mathbf{x} = \boldsymbol{\chi}(\mathbf{X}). \tag{1}$$

The deformation gradient is defined as

$$\mathbf{F} = \frac{\partial \boldsymbol{\chi}(\mathbf{X})}{\partial \mathbf{X}}. \tag{2}$$

The ratio between the volumes in the current and reference configurations is $J \equiv \det\mathbf{F} > 0$.

We consider a quasi-static deformation in the absence of a magnetic field, electrical charges or electric currents within the material. Consequently, Maxwell equations take the form

$$\mathrm{Div}\mathbf{D}^0 = 0 \quad \text{and} \quad \mathrm{Curl}\mathbf{E}^0 = 0, \tag{3}$$

where $\mathbf{D}^0$ is the electric displacement and $\mathbf{E}^0$ is the electric field in the reference configuration. Note that $\mathrm{Div}(\cdot)$ and $\mathrm{Curl}(\cdot)$ are the differential operators in the reference configuration, while $\mathrm{div}(\cdot)$ and $\mathrm{curl}(\cdot)$ denote the corresponding differential operators in the current configuration. The referential electric field and electric displacement are related to their counterpart in the deformed configuration (Dorfmann and Ogden, 2005, 2010) via

$$\mathbf{E}^0 = \mathbf{F}^{\mathrm{T}}\mathbf{E} \quad \text{and} \quad \mathbf{D}^0 = J\mathbf{F}^{-1}\mathbf{D}. \tag{4}$$

We follow the analysis proposed by Dorfmann and Ogden (2005, 2010) and consider the elastic dielectrics whose constitutive relation is given in terms of a scalar-valued energy-density function $\Psi(\mathbf{F}, \mathbf{E}^0)$ such that

$$\mathbf{P} = \frac{\partial \Psi(\mathbf{F}, \mathbf{E}^0)}{\partial \mathbf{F}} \quad \text{and} \quad \mathbf{D}^0 = -\frac{\partial \Psi(\mathbf{F}, \mathbf{E}^0)}{\partial \mathbf{E}^0}, \tag{5}$$

where $\mathbf{P}$ is the total nominal stress tensor. The corresponding equations for an incompressible material are

$$\mathbf{P} = \frac{\partial \Psi(\mathbf{F}, \mathbf{E}^0)}{\partial \mathbf{F}} - p\mathbf{F}^{-T} \quad \text{and} \quad \mathbf{D}^0 = -\frac{\partial \Psi(\mathbf{F}, \mathbf{E}^0)}{\partial \mathbf{E}^0}, \tag{6}$$

where p is an unknown Lagrange multiplier. For an isotropic electroelastic material, an energy-density function Ψ can be expressed as a function of the six invariants

$$\Psi\left(\mathbf{F}, \mathbf{E}^0\right) = \Psi(I_1, I_2, I_3, I_{4e}, I_{5e}, I_{6e}), \tag{7}$$

where

$$I_1 = \mathrm{Tr}\mathbf{C}, \quad I_2 = \frac{1}{2}\left(I_1^2 - \mathrm{Tr}\mathbf{C}^2\right), \quad I_3 = \det\mathbf{C}, \tag{8}$$

$$I_{4e} = \mathbf{E}^0 \cdot \mathbf{E}^0, \quad I_{5e} = \mathbf{E}^0 \cdot \mathbf{C}^{-1}\mathbf{E}^0, \quad I_{6e} = \mathbf{E}^0 \cdot \mathbf{C}^{-2}\mathbf{E}^0, \tag{9}$$

where $\mathbf{C} = \mathbf{F}^T\mathbf{F}$ is the right Cauchy-Green strain tensor. In the absence of body forces the equilibrium equation takes the form

$$\mathrm{Div}\mathbf{P} = 0. \tag{10}$$

The equilibrium equation in the *current* configuration is

$$\mathrm{div}\mathbf{T} = 0, \tag{11}$$

where the Cauchy stress tensor is related to the first Piola-Kirchhoff stress tensor via $\mathbf{T} = J^{-1}\mathbf{P}\mathbf{F}^T$.

Next we analyze small amplitude perturbations *superimposed* on the finitely deformation and electric field (Dorfmann and Ogden, 2010). The corresponding incremental equations are

$$\mathrm{Div}\dot{\mathbf{P}} = 0, \quad \mathrm{Div}\dot{\mathbf{D}}^0 = 0 \quad \text{and} \quad \mathrm{Curl}\dot{\mathbf{E}}^0 = 0, \tag{12}$$

where $\dot{\mathbf{P}}$, $\dot{\mathbf{D}}^0$ and $\dot{\mathbf{E}}^0$ are incremental changes in $\mathbf{P}$, $\mathbf{D}^0$ and $\mathbf{E}^0$, respectively. The linearized expressions for the incremental changes in the nominal stress tensor and electric displacement are

$$\dot{P}_{ij} = \mathscr{A}^0_{ijkl}\dot{F}_{kl} + \mathscr{G}^0_{ijk}\dot{E}^0_k \quad \text{and} \quad -\dot{D}^0_i = \mathscr{G}^0_{jki}\dot{F}_{jk} + \mathscr{E}^0_{ij}\dot{E}^0_j, \tag{13}$$

where the tensors of the electroelastic moduli are defined as

$$\mathscr{A}^0_{i\alpha k\beta} = \frac{\partial^2\Psi}{\partial F_{i\alpha}\partial F_{k\beta}}, \quad \mathscr{G}^0_{i\alpha\beta} = \frac{\partial^2\Psi}{\partial F_{i\alpha}\partial E^0_\beta} \quad \text{and} \quad \mathscr{E}^0_{\alpha\beta} = \frac{\partial^2\Psi}{\partial E^0_\alpha \partial E^0_\beta}. \tag{14}$$

In general, the electroelastic moduli are functions of the applied finite deformation and electric field, namely, $\mathscr{A}^{\mathbf{0}} = \mathscr{A}^{\mathbf{0}}(\mathbf{F}, \mathbf{E}^0)$, $\mathscr{G}^{\mathbf{0}} = \mathscr{G}^{\mathbf{0}}(\mathbf{F}, \mathbf{E}^0)$, and $\mathscr{E}^{\mathbf{0}} = \mathscr{E}^{\mathbf{0}}(\mathbf{F}, \mathbf{E}^0)$, and the specific dependence is defined by the choice of the energy-density function $\Psi(\mathbf{F}, \mathbf{E}^0)$. For an incompressible material, equation $(13)_1$ modifies as

$$\dot{P}_{ij} = \mathscr{A}^0_{ijkl}\dot{F}_{kl} + \mathscr{G}^0_{ijk}\dot{E}^0_k - \dot{p}F^{-1}_{ji} + pF^{-1}_{jk}\dot{F}_{kl}F^{-1}_{li}, \tag{15}$$

where $\dot{p}$ is an incremental change in p. The components of the electroelastic moduli in the current and reference configurations are related via

$$\mathscr{A}_{ijkl} = J^{-1}F_{j\alpha}F_{l\beta}\mathscr{A}^0_{i\alpha k\beta}, \quad \mathscr{G}_{ijk} = J^{-1}F_{j\alpha}F_{k\beta}\mathscr{G}^0_{i\alpha\beta} \quad \text{and} \quad \mathscr{E}_{ij} = J^{-1}F_{i\alpha}F_{j\beta}\mathscr{E}^0_{\alpha\beta}. \tag{16}$$

It can be shown that these tensors of electroelastic moduli possess the symmetries

$$\mathscr{A}_{ijkl} = \mathscr{A}_{klij}, \quad \mathscr{G}_{ijk} = \mathscr{G}_{jik} \quad \text{and} \quad \mathscr{E}_{ij} = \mathscr{E}_{ji}. \tag{17}$$

Let $\dot{\mathbf{T}}$, $\dot{\mathbf{D}}$ and $\dot{\mathbf{E}}$ denote the 'push-forward' counterparts of $\dot{\mathbf{P}}$, $\dot{\mathbf{D}}^0$ and $\dot{\mathbf{E}}^0$, respectively. These incremental changes are given by

$$\dot{\mathbf{T}} = J^{-1}\dot{\mathbf{P}}\mathbf{F}^T, \quad \dot{\mathbf{D}} = J^{-1}\mathbf{F}\dot{\mathbf{D}}^0 \quad \text{and} \quad \dot{\mathbf{E}} = \mathbf{F}^{-T}\dot{\mathbf{E}}^0. \tag{18}$$

We introduce the notation for the incremental displacement $\mathbf{v} = \dot{\mathbf{x}}$ and recall that $\dot{\mathbf{F}} = (\mathrm{grad}\,\mathbf{v})\mathbf{F}$. By substitution of (15) and (16) into (18), we obtain

$$\dot{T}_{ij} = \mathscr{A}_{ijkl}v_{k,l} + \mathscr{G}_{ijk}\dot{E}_k - \dot{p}\delta_{ij} + pv_{j,i} \quad \text{and} \quad -\dot{D}_i = \mathscr{G}_{jki}v_{j,k} + \mathscr{E}_{ij}\dot{E}_j. \tag{19}$$

In the current configuration the incremental equations (12) take the form

$$\mathrm{div}\dot{\mathbf{T}} = 0, \quad \mathrm{div}\dot{\mathbf{D}} = 0 \quad \text{and} \quad \mathrm{curl}\dot{\mathbf{E}} = 0. \tag{20}$$

By using equations (19), $(20)_1$ and $(20)_2$ we obtain

$$\mathscr{A}_{ijkl}v_{k,lj} + \mathscr{G}_{ijk}\dot{E}_{k,j} - \dot{p}_{,i} = 0 \quad \text{and} \quad \mathscr{G}_{jki}v_{j,ki} + \mathscr{E}_{ij}\dot{E}_{j,i} = 0. \tag{21}$$

We seek a solution for equation (21) in the form

$$v_i = \tilde{v}_i f(\hat{\mathbf{a}}\cdot\mathbf{x}), \quad \dot{p} = \tilde{q}f'(\hat{\mathbf{a}}\cdot\mathbf{x}), \quad \dot{E}_i = \tilde{e}_i f'(\hat{\mathbf{a}}\cdot\mathbf{x}), \tag{22}$$

where f is a continuous and sufficiently differentiable function, $\hat{\mathbf{a}} = a_1\bar{\mathbf{e}}_1 + a_2\bar{\mathbf{e}}_2 + a_3\bar{\mathbf{e}}_3$ is a unit vector; $\tilde{v}_i$, $\tilde{e}_i$ and $\tilde{q}$ are incremental macroscopic quantities independent of $\mathbf{x}$.

Next, we restrict our attention to a 2D setting. For this specification, we follow the stability analysis presented in Rudykh et al. (2014). In particular, for the plane problem we assume the absence of an electric field in the $\mathbf{X}_3$ direction, therefore equation $(20)_3$ reduces to

$$\dot{E}_{2,1} - \dot{E}_{1,2} = 0. \tag{23}$$

By using $(22)_3$ together with (23), we find that

$$\tilde{e}_1 = \xi^{-1}\tilde{e}_2, \tag{24}$$

where $\xi \equiv a_2/a_1$. Next, we recall that the incompressibility constraint implies that $\mathrm{div}\,\mathbf{v} = v_{1,1} + v_{2,2} = 0$. Then, from $(22)_1$ we have

$$\tilde{v}_1 = -\xi\tilde{v}_2. \tag{25}$$

Substituting equations (22), (24) and (25) into (21), we obtain the sextic polynomial equation

$$\Gamma_6\xi^6 + \Gamma_5\xi^5 + \Gamma_4\xi^4 + \Gamma_3\xi^3 + \Gamma_2\xi^2 + \Gamma_1\xi + \Gamma_0 = 0, \tag{26}$$

where the coefficients Γ_i are given by

$$\begin{aligned}
\Gamma_0 &= \mathscr{G}^2_{121} - \mathscr{A}_{2121}\mathscr{E}_{11},\\
\Gamma_1 &= 2(-\mathscr{A}_{2121}\mathscr{E}_{12} + (\mathscr{A}_{1121} - \mathscr{A}_{2122})\mathscr{E}_{11} + \mathscr{G}_{121}(\mathscr{G}_{221} + \mathscr{G}_{122} - \mathscr{G}_{111})),\\
\Gamma_2 &= -\mathscr{A}_{2121}\mathscr{E}_{22} + 4(\mathscr{A}_{1121} - \mathscr{A}_{2122})\mathscr{E}_{12} - (\mathscr{A}_{1111} - 2\mathscr{A}_{1122} - 2\mathscr{A}_{1221} + \mathscr{A}_{2222})\mathscr{E}_{11} - 2\mathscr{G}_{121}(\mathscr{G}_{112} + \mathscr{G}_{121} - \mathscr{G}_{222})\\
&\quad + (\mathscr{G}_{122} + \mathscr{G}_{221} - \mathscr{G}_{111})^2,\\
\Gamma_3 &= -2((\mathscr{A}_{1112} - \mathscr{A}_{1222})\mathscr{E}_{11} + (\mathscr{A}_{1111} - 2\mathscr{A}_{1122} - 2\mathscr{A}_{1221} + \mathscr{A}_{2222})\mathscr{E}_{12} + (\mathscr{A}_{2122} - \mathscr{A}_{1121})\mathscr{E}_{22}\\
&\quad + (\mathscr{G}_{121}\mathscr{G}_{122} - (\mathscr{G}_{111} - \mathscr{G}_{122} - \mathscr{G}_{221})(\mathscr{G}_{112} + \mathscr{G}_{121} - \mathscr{G}_{222})))\\
\Gamma_4 &= -(\mathscr{A}_{1111} - 2\mathscr{A}_{1122} - 2\mathscr{A}_{1221} + \mathscr{A}_{2222})\mathscr{E}_{22} - 4(\mathscr{A}_{1112} - \mathscr{A}_{1222})\mathscr{E}_{12} - \mathscr{A}_{1212}\mathscr{E}_{11} + (\mathscr{G}_{112} + \mathscr{G}_{121} - \mathscr{G}_{222})^2\\
&\quad + 2\mathscr{G}_{122}(\mathscr{G}_{111} - \mathscr{G}_{122} - \mathscr{G}_{221}),\\
\Gamma_5 &= 2((\mathscr{A}_{1222} - \mathscr{A}_{1112})\mathscr{E}_{22} - \mathscr{A}_{1212}\mathscr{E}_{12} + \mathscr{G}_{122}(\mathscr{G}_{112} + \mathscr{G}_{121} - \mathscr{G}_{222})), \Gamma_6 = \mathscr{G}^2_{122} - \mathscr{A}_{1212}\mathscr{E}_{22}.
\end{aligned} \tag{27}$$

The existence of a non-trivial real solution of the polynomial equation (26) is associated with the onset of instability along an electromechanical loading path. In the following, equation (26) serves as the onset of instability condition for considered DE composites.

3. Analysis

In this section we present the analysis for determining the onset

of electromechanical instabilities in periodic composites undergoing finite deformations in the presence of an electric field. We note that the critical condition (26) can be used to determine the onset of instabilities in multiphase hyperelastic dielectrics (Rudykh et al., 2014). The analysis is implemented in the finite element code COMSOL Multiphysics.

The energy-density function of an n-phase composite is

$$\Psi\left(\overline{\mathbf{F}},\mathbf{X},\overline{\mathbf{E}}^0\right)=\sum_{r=1}^{n}\varphi^{(r)}(\mathbf{X})\Psi^{(r)}\left(\mathbf{F},\mathbf{E}^0\right) \tag{28}$$

where

$$\varphi^{(r)}(\mathbf{X})=\begin{cases}1, & \text{if } \mathbf{X}\in\mathscr{B}_0^{(r)};\\ 0, & \text{otherwise},\end{cases} \tag{29}$$

The volume fraction of the r-phase is

$$c^{(r)}=\int_{\mathscr{B}_0}\varphi^{(r)}(\mathbf{X})dV. \tag{30}$$

The volume fractions are related via

$$\sum_{r=1}^{n}c^{(r)}=1. \tag{31}$$

We impose homogeneous boundary conditions $\mathbf{x}=\mathbf{F}_0\mathbf{X}$ on the boundary of the composite $\partial\mathscr{B}_0$, where $\mathbf{F}_0$ is a constant tensor with $\det\mathbf{F}_0>0$ (Hill, 1972; Ogden, 1974). It can be shown that the average deformation gradient

$$\overline{\mathbf{F}}\equiv\frac{1}{V}\int_{\mathscr{B}_0}\mathbf{F}(\mathbf{X})dV=\mathbf{F}_0. \tag{32}$$

The average 1^{st} Piola-Kirchhoff stress tensor, electric displacement and electric field are

$$\overline{\mathbf{P}}=\frac{1}{V}\int_{\mathscr{B}_0}\mathbf{P}(\mathbf{X})dV,\quad \overline{\mathbf{D}}^0=\frac{1}{V}\int_{\mathscr{B}_0}\mathbf{D}^0(\mathbf{X})dV\quad\text{and}\quad\overline{\mathbf{E}}^0=\frac{1}{V}\int_{\mathscr{B}_0}\mathbf{E}^0(\mathbf{X})dV, \tag{33}$$

respectively. In the 2-D case the integration is performed over the area of a periodic unit cell, which occupies the domain

$$0\le X_1\le b\quad\text{and}\quad 0\le X_2\le a \tag{34}$$

in the reference configuration.

In our finite element numerical simulations, the macroscopic electro-mechanical loading conditions are applied in terms of periodic boundary conditions of displacement (u_1,u_2) and electric potential (U). A representetive 2-D unit cell of a periodic composite is shown in Fig.1. These periodic boundary conditions are:

The top $(X_2=a)$ and bottom $(X_2=0)$ sides are related via

$$\begin{cases}u_2^B=u_2^T+(\overline{F}_{22}-1)a,\\ u_1^B=u_1^T+\overline{F}_{12}a,\\ U^B(X_1,0)=U^T(X_1,a)+\overline{E}_2^0a.\end{cases} \tag{35}$$

The right $(X_1=b)$ and left $(X_1=0)$ sides are related via

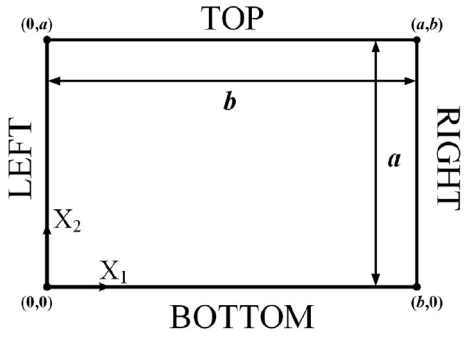

Fig. 1. Schematic representation of two-dimensional rectangular unit cell.

$$\begin{cases}u_1^L=u_1^R+(\overline{F}_{11}-1)b,\\ u_2^L=u_2^R+\overline{F}_{21}b,\\ U^L(0,X_2)=U^R(b,X_2)+\overline{E}_1^0b.\end{cases} \tag{36}$$

The application of the periodic boundary conditions allows us to determine the solution along the electro-mechanical loading path. For simplicity, here we consider the electromechanical loading defined as

$$\overline{\mathbf{F}}=\overline{\lambda}\mathbf{e}_1\otimes\mathbf{e}_1+\overline{\lambda}^{-1}\mathbf{e}_2\otimes\mathbf{e}_2+\mathbf{e}_3\otimes\mathbf{e}_3\quad\text{and}\quad\overline{\mathbf{E}}^0=\overline{E}_1^0\mathbf{e}_1+\overline{E}_2^0\mathbf{e}_2. \tag{37}$$

We note that the deformation gradient defined in equation (37) does not include macroscopic shear modes of deformation. For stability consideration of a more general deformation including non-zero shear terms, the average deformation gradient with non-zero shear components needs to be transformed into the corresponding diagonal average deformation gradient defined in equation (37) by choosing the corresponding principal coordinate system. Thus, the components of the electromechanical tensors are to be evaluated in this principal coordinate system; and the macroscopic stability analysis is performed in terms of the moduli calculated in the new principal coordinate system. For simplicity, in this study we restrict our analysis to the case when the average deformation gradient is prescribed by equation (37).

The average response of the periodic composites is calculated by integration over the corresponding unit cell as in $(33)_1$ and $(33)_2$. The primary solution is valid until a possible instability point along the electromechanical loading.

To identify the onset of the coupled electromechanical instabilities, we utilize the critical condition (26). The analysis of the electromechanical stability of DE composites requires determination of the instantaneous tensors of the electroelastic moduli $\mathscr{A}_{ijkl}$, $\mathscr{G}_{ijk}$ and $\mathscr{E}_{ij}$. To this end we use a numerical perturbation technique (see for example for the mechanical case (Riks, 1984; Ecer, 1973; Hangai and Kawamata, 1972)). In particular, we perform a set of incremental changes in deformation and electric field from a finitely deformed state in the presence of an electric field. These incremental changes lead to a macroscopic response of the DE composite, resulting in variations in the average nominal stress and electric displacement. We perform the following five small amplitude numerical tests, namely

$$\overline{\mathbf{F}}^{[1]}=\overline{\lambda}\mathbf{e}_1\otimes\mathbf{e}_1+\delta\overline{\gamma}\mathbf{e}_1\otimes\mathbf{e}_2+\overline{\lambda}^{-1}\mathbf{e}_2\otimes\mathbf{e}_2\quad\text{and}\quad\overline{\mathbf{F}}^{[2]}=\overline{\lambda}\mathbf{e}_1\otimes\mathbf{e}_1+\overline{\lambda}^{-1}\mathbf{e}_2\otimes\mathbf{e}_2+\delta\overline{\gamma}\mathbf{e}_2\otimes\mathbf{e}_1, \tag{38}$$

$$\overline{\mathbf{F}}^{[3]}=\left(\overline{\lambda}+\delta\overline{\lambda}\right)\mathbf{e}_1\otimes\mathbf{e}_1+\left(\overline{\lambda}+\delta\overline{\lambda}\right)^{-1}\mathbf{e}_2\otimes\mathbf{e}_2, \tag{39}$$

$$\overline{\mathbf{E}}^{0[1]} = \left(\overline{E}_1^0 + \delta\overline{E}\right)\mathbf{e}_1 + \overline{E}_2^0\mathbf{e}_2 \quad \text{and} \quad \overline{\mathbf{E}}^{0[2]} = \overline{E}_1^0\mathbf{e}_1 + \left(\overline{E}_2^0 + \delta\overline{E}\right)\mathbf{e}_2, \tag{40}$$

where $\delta\overline{\gamma}$, $\delta\overline{\lambda}$ and $\delta\overline{E}$ are sufficiently small quantities. By performing these tests and calculating the corresponding changes in the first Piola-Kirchhoff stress tensor and in the referential electric displacement, the electroelastic moduli in the reference configuration are determined through the use of relations (13). The corresponding equations for the electroelastic moduli are

$$\mathscr{A}^0_{ijkl} = \frac{\delta\overline{P}^{[m,0]}_{ij}}{\delta\overline{F}^{[m]}_{kl}} = \frac{\left(\overline{\mathbf{P}}\left(\overline{\mathbf{F}}^{[m]}, \overline{\mathbf{E}}^0\right) - \overline{\mathbf{P}}\left(\overline{\mathbf{F}}, \overline{\mathbf{E}}^0\right)\right)_{ij}}{\left(\overline{\mathbf{F}}^{[m]} - \overline{\mathbf{F}}\right)_{kl}} = \frac{\left(\overline{\mathbf{P}}\left(\overline{\mathbf{F}}^{[m]}, \overline{\mathbf{E}}^0\right) - \overline{\mathbf{P}}\left(\overline{\mathbf{F}}, \overline{\mathbf{E}}^0\right)\right)_{ij}}{\delta\overline{\gamma}}, k \neq l, m = 1, 2; \tag{41}$$

$$\mathscr{G}^0_{ijk} = \frac{\delta\overline{P}^{[0,n]}_{ij}}{\delta\overline{E}^{0[n]}_k} = \frac{\left(\overline{\mathbf{P}}\left(\overline{\mathbf{F}}, \overline{\mathbf{E}}^{0[n]}\right) - \overline{\mathbf{P}}\left(\overline{\mathbf{F}}, \overline{\mathbf{E}}^0\right)\right)_{ij}}{\left(\overline{\mathbf{E}}^{0[n]} - \overline{\mathbf{E}}^0\right)_k} = \frac{\left(\overline{\mathbf{P}}\left(\overline{\mathbf{F}}, \overline{\mathbf{E}}^{0[n]}\right) - \overline{\mathbf{P}}\left(\overline{\mathbf{F}}, \overline{\mathbf{E}}^0\right)\right)_{ij}}{\delta\overline{E}}, n = 1, 2; \tag{42}$$

$$\mathscr{E}^0_{ij} = -\frac{\delta\overline{D}^{0[0,n]}_i}{\delta\overline{E}^{0[n]}_j} = -\frac{\left(\overline{\mathbf{D}}^0\left(\overline{\mathbf{F}}, \overline{\mathbf{E}}^{0[n]}\right) - \overline{\mathbf{D}}^0\left(\overline{\mathbf{F}}, \overline{\mathbf{E}}^0\right)\right)_i}{\left(\overline{\mathbf{E}}^{0[n]} - \overline{\mathbf{E}}^0\right)_j} = -\frac{\left(\overline{\mathbf{D}}^0\left(\overline{\mathbf{F}}, \overline{\mathbf{E}}^{0[n]}\right) - \overline{\mathbf{D}}^0\left(\overline{\mathbf{F}}, \overline{\mathbf{E}}^0\right)\right)_i}{\delta\overline{E}}, n = 1, 2. \tag{43}$$

Note that in equation (41) only shear tests $\overline{\mathbf{F}}^{[1]}$ and $\overline{\mathbf{F}}^{[2]}$ are applied, consequently $m = 1, 2$. To determine the components of electroelastic moduli $\mathscr{A}^0_{ijkk}$ (no summation), $i \neq j$, we use the symmetry $\mathscr{A}^0_{ijkk} = \mathscr{A}^0_{kkij}$ and apply equation (41) again. However, when $i = j$ and $k = l$, the components $\mathscr{A}^0_{iikk}$ (no summation) cannot be determined from the tension test (39). This is due to the fact that the following equation system stemming from equation (13)

$$\begin{cases} \delta\overline{P}^{[3,0]}_{11} = \mathscr{A}^0_{1111}\delta\overline{F}^{[3]}_{11} + \mathscr{A}^0_{1122}\delta\overline{F}^{[3]}_{22}, \\ \delta\overline{P}^{[3,0]}_{22} = \mathscr{A}^0_{2211}\delta\overline{F}^{[3]}_{11} + \mathscr{A}^0_{2222}\delta\overline{F}^{[3]}_{22}, \end{cases} \tag{44}$$

does not have a solution for $\mathscr{A}^0_{1111}$, $\mathscr{A}^0_{2222}$, and $\mathscr{A}^0_{1122} = \mathscr{A}^0_{2211}$. Clearly, it is impossible to fully characterize the elastic properties of a material on the basis of plane tests alone (Ogden, 2008). However, the corresponding coefficients in the critical condition for the onset of instabilities (26) can be fully determined through certain combinations of the terms $\mathscr{A}^0_{iikk}$ (no summation). These combinations can be obtained from the information provided by the tension test (39). The incompressibility constraint implies

$$\delta\overline{\mathbf{F}} : \overline{\mathbf{F}}^{-T} = 0. \tag{45}$$

For the tension test (39), the incompressibility constraint reads

$$\delta\overline{F}^{[3]}_{11} = -\delta\overline{F}^{[3]}_{22}\frac{\overline{F}_{11}}{\overline{F}_{22}} = -\frac{\delta\overline{F}^{[3]}_{22}}{\left(\overline{F}_{22}\right)^2}. \tag{46}$$

Thus, the combinations $(\mathscr{A}^0_{2222} - \mathscr{A}^0_{2211})$ and $(\mathscr{A}^0_{1111} - \mathscr{A}^0_{2211})$ can be determined by applying the tension test (39) together with $(16)_1$, (44) and (46). In particular, we obtain

$$\begin{aligned} \mathscr{A}^0_{2222} - \mathscr{A}^0_{2211} &= \overline{F}_{22}\overline{F}_{22}\mathscr{A}_{2222} - \overline{F}_{22}\overline{F}_{11}\mathscr{A}_{2211} \\ &= \overline{F}^2_{22}\left(\mathscr{A}_{2222} - \mathscr{A}_{2211}\overline{F}_{11}/\overline{F}_{22}\right) \\ &= \overline{F}^2_{22}\delta\overline{P}^{[3,0]}_{22}\Big/\delta\overline{F}^{[3]}_{22}, \end{aligned} \tag{47}$$

and

$$\begin{aligned} \mathscr{A}^0_{1111} - \mathscr{A}^0_{2211} &= \overline{F}_{11}\overline{F}_{11}\mathscr{A}_{1111} - \overline{F}_{22}\overline{F}_{11}\mathscr{A}_{2211} \\ &= \overline{F}^2_{11}\left(\mathscr{A}_{1111} - \mathscr{A}_{2211}\overline{F}_{22}/\overline{F}_{11}\right) \\ &= \overline{F}^2_{11}\delta\overline{P}^{[3,0]}_{11}\Big/\delta\overline{F}^{[3]}_{11}, \end{aligned} \tag{48}$$

where $\delta\overline{P}^{[3,0]}_{ii} = (\overline{\mathbf{P}}(\overline{\mathbf{F}}^{[3]}, \overline{\mathbf{E}}^0) - \overline{\mathbf{P}}(\overline{\mathbf{F}}, \overline{\mathbf{E}}^0))_{ii}$, no summation.

By utilizing equations (16), (17), (27), (41–43), (47), (48) and (27), all the components of the electro-elastic tensors required for calculating of the coefficients Γ_i can be determined. To perform the stability analysis, we implement these equations in our MATLAB code to evaluate the components of electroelastic moduli from the numerical tests, and, then, to check the condition for the onset of instability (26) at each point of the electromechanical loading path. Thus, the critical stretch and electric field are determined. Results of the stability analysis of specific periodic DE composites are discussed in the next section.

4. Results

The stability analysis presented in Sec. 3 is rather generic, however, in this section the examples are presented for DE composites which phases are described by an ideal dielectric elastomer model. The corresponding energy-density function is

$$\Psi^{(r)}\left(\mathbf{F}, \mathbf{E}^0\right) = \frac{\mu^{(r)}}{2}(\mathrm{Tr}\mathbf{C} - 3) - \frac{\varepsilon_0\varepsilon^{(r)}J}{2}\mathbf{E}^0\mathbf{C}^{-1}\mathbf{E}^0 - \mu^{(r)}\ln J + \frac{\Lambda^{(r)}}{2}(J-1)^2, \tag{49}$$

where μ is the shear modulus and Λ is the Lamé's first parameter, ε_0 is the permittivity of vacuum, and ε is the relative permittivity. In the numerical simulations, we maintain the nearly incompressible behavior of the phases by assigning a high ratio between the first Lamé parameter and shear modulus, in particular, $\Lambda^{(r)}/\mu^{(r)} = 100$. Note that the macroscopic deformation is enforced to be incompressible, while locally the materials are allowed to develop some compressible (nearly incompressible) deformations.

To determine the response of periodic DE composites prior to instability, we utilize (35) and (36) to impose the periodic boundary conditions on a unit cell. The equilibrium equation and the Maxwells equations are solved separately in the FE code COMSOL Multiphysics, and the electromechanical coupling is established via the dependence of the resulting total stress on the electric field, while the Maxwells equations are solved in the current configuration, which is a result of deformations. The resulting output is calculated in terms of the average nominal stress tensor $(33)_1$ and electric displacement $(33)_2$. By performing the small amplitude numerical tests (38–40) and making use of relations (41–43), (47) and (48), we determine the electroelastic moduli in the reference configuration. Then, the counterparts of the electroelastic moduli in the current configuration are evaluated by using equation (16). To determine the critical stretch $\overline{\lambda}_c$, we check the condition for the onset of macroscopic instability (26) at each point of the electromechanical loading path (37).

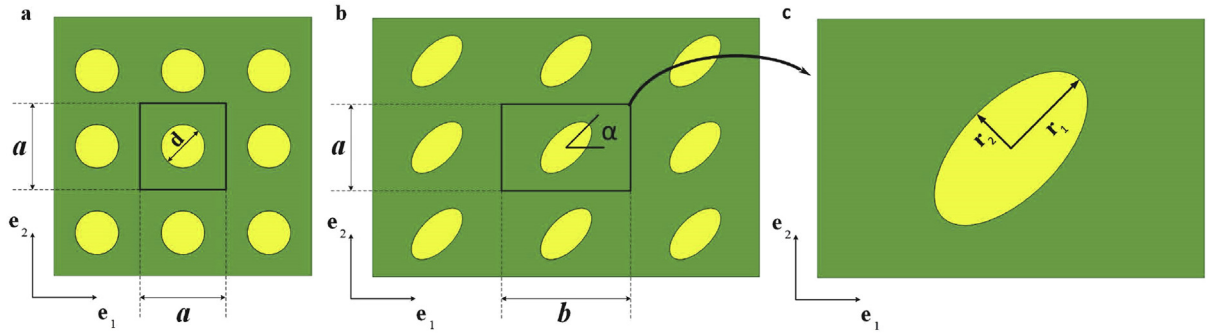

Fig. 2. Schematic representation of DE composites with square and rectangular periodic microstructures with circular (a) and elliptical (b) inclusions; the periodic unit cell (c).

4.1. DE composites with periodically distributed circular inclusions

We examine the response of DE composites with periodically distributed circular particles embedded in a soft matrix. Fig. 2(a) shows a representative 2-D periodic composite with a square periodic unit cell of circular inclusions embedded in a matrix. The contrasts in the shear moduli and relative permittivities of the phases are $k_\mu = \mu^{(i)}/\mu^{(m)}$ and $k_\varepsilon = \varepsilon^{(i)}/\varepsilon^{(m)}$, where superscripts (i) and (m) correspond to the inclusion and matrix, respectively. The average dimensionless electric fields are $\widehat{\mathbf{E}}^0 = \overline{\mathbf{E}}^0\sqrt{\varepsilon_0\overline{\varepsilon}/\overline{\mu}}$ (where $\overline{\varepsilon} = c^{(m)}\varepsilon^{(m)} + c^{(i)}\varepsilon^{(i)}$ and $\overline{\mu} = c^{(m)}\mu^{(m)} + c^{(i)}\mu^{(i)}$) and $\tilde{\mathbf{E}}^0 = \overline{\mathbf{E}}^0\sqrt{\varepsilon_0\varepsilon^{(m)}/\mu^{(m)}}$. The volume fraction of the inclusion phase is defined by $c^{(i)} = \pi d^2/4a^2$.

We start from considering the macroscopic response of the periodic DE composites. Fig. 3 shows the dependence of the mean deviatoric part of the normalized Cauchy stress, $\overline{\boldsymbol{\sigma}}' = \mathrm{dev}\overline{\boldsymbol{\sigma}}/\mu^{(m)}$ as a function of the stretch ratio for different values and directions of the

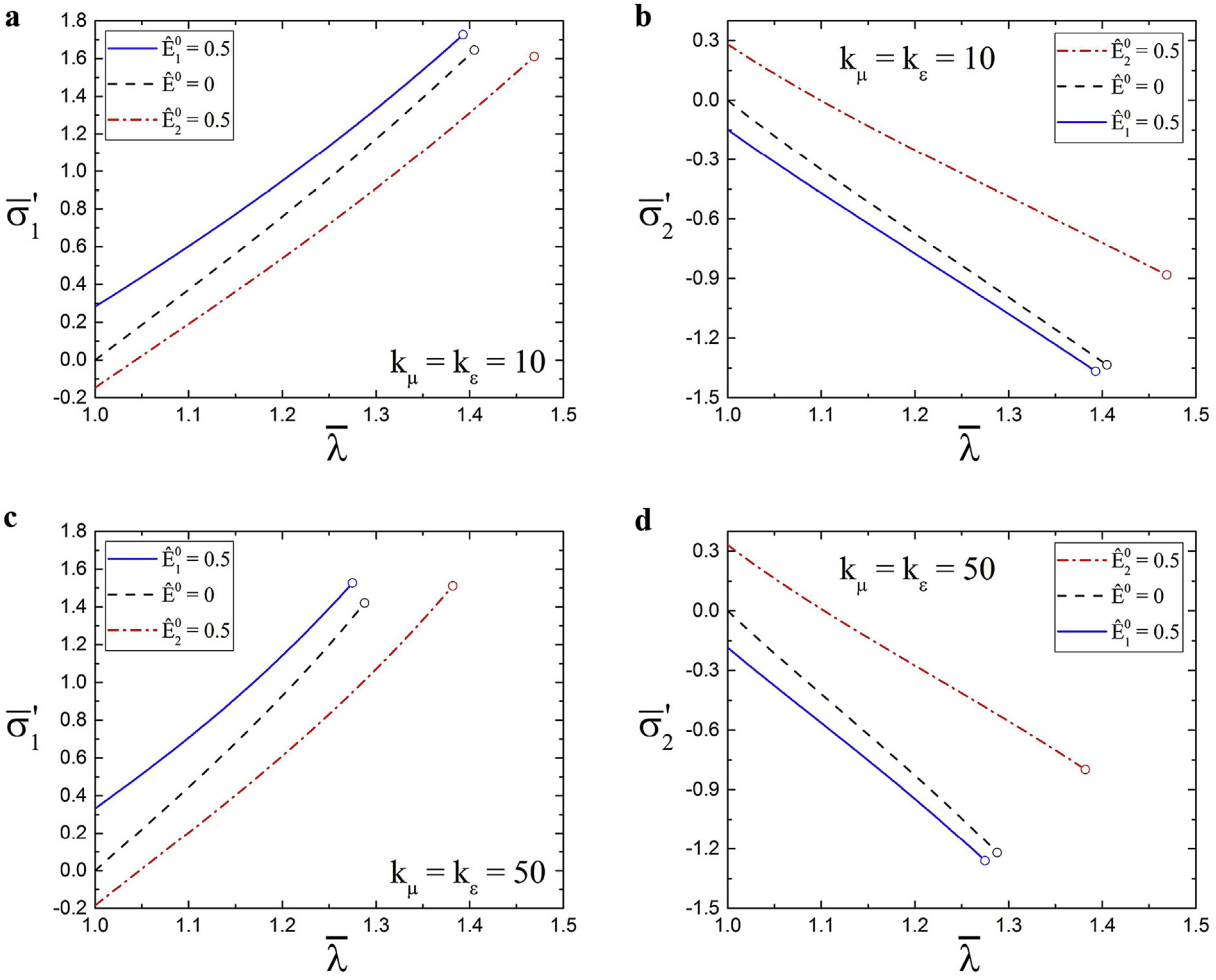

Fig. 3. Normalized deviatoric Cauchy stress vs stretch ratio for DE composites with the contrasts in the shear moduli and relative permittivities $k_\mu = k_\varepsilon = 10$ ((a),(b)) and $k_\mu = k_\varepsilon = 50$ ((c),(d)). The volume fraction of the inclusion phase is $c^{(i)} = 0.283$ (corresponds to the diameter $d = 0.6$).

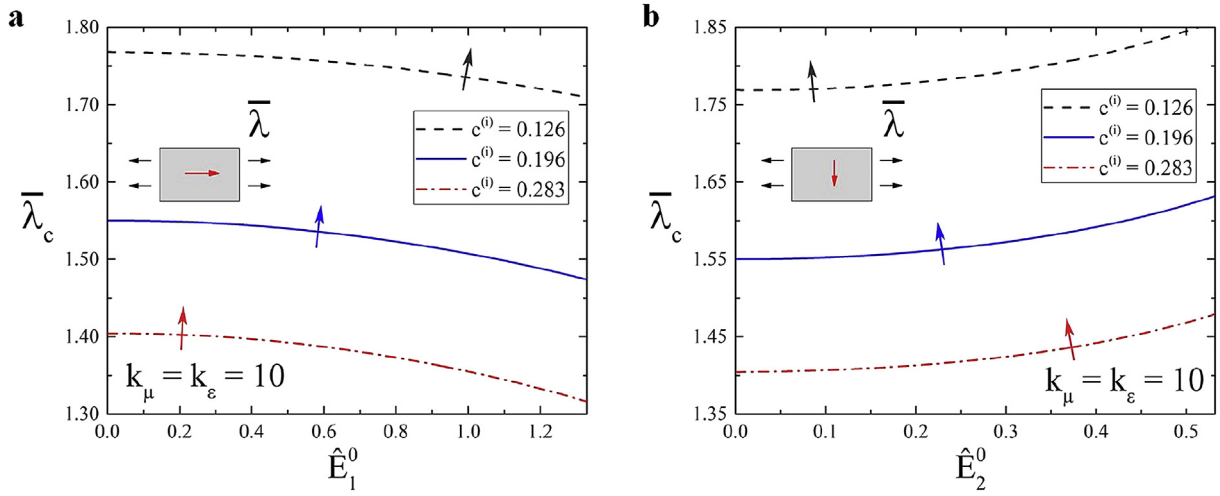

Fig. 4. Critical stretch ratio vs electric field for DE composites with the contrasts in the shear moduli and relative permittivities $k_\mu = k_\varepsilon = 10$. (a) - the electric field is aligned with the stretch direction, (b) - the electric field applied perpendicularly to the stretch direction.

applied electric field. The results are shown for DE composites with the contrasts in the shear moduli and relative permittivities $k_\mu = k_\varepsilon = 10$ (Fig. 3(a) and (b)) and $k_\mu = k_\varepsilon = 50$ (Fig. 3(c) and (d)). The composite volume fraction is $c^{(i)} = 0.283$ (corresponds to the diameter $d = 0.6a$). The stress-stretch behavior for the purely mechanical case (in the absence of an electric field, $\hat{E}^0 = 0$) is denoted by dashed curves. The continuous curve corresponds to the response of the DE composites subjected to an electric field of magnitude $\hat{E}_1^0 = 0.5$; the applied electric field is aligned with the stretch direction ($\mathbf{e}_1$). The dash-dotted curve represents the response of the DE composites in the presence of an electric field applied perpendicularly to the stretch direction, $\mathbf{E} = \hat{E}_2^0 \mathbf{e}_2$ with $\hat{E}_2^0 = 0.5$. The values of the critical stretches corresponding to the onset of instability are denoted by circles. We observe that $\overline{\sigma}_1{}'(\overline{\lambda})$ is a monotonically increasing function of $\overline{\lambda}$, while $\overline{\sigma}_2{}'(\overline{\lambda})$ is a decreasing function. Clearly, the associate electrical stresses in the unit cell depend on the *spatial* electric field and the effective permittivity. Meanwhile, $\mathbf{e}_1$ and $\mathbf{e}_2$ components of the average electric field in the current configuration depend on the stretch as $\overline{E}_1 = \overline{\lambda}^{-1}\overline{E}_1^0$ and $\overline{E}_2 = \overline{\lambda}\overline{E}_2^0$. The effective permittivity $\tilde{\varepsilon}_{11}$ is a decreasing function of the stretch ratio, while $\tilde{\varepsilon}_{22}$ is a monotonic increasing function of the stretch ratio.[1] This, together, with the fact that $\overline{E}_1$ decreases and $\overline{E}_2$ increases with an increase in $\overline{\lambda}$, results in the observed behavior of the stress-stretch curves in Fig. 3. In particular, the corresponding continuous curves approach the dashed ones with an increase in $\overline{\lambda}$, while the dash-dotted curves shift away from the dashed ones with an increase in the applied stretch.

Next we examine the stability of the DE periodic composites along the applied electromechanical loading (39). The dependence of the critical stretch on the electric field is shown in Fig. 4 for the composite with the contrasts in the shear moduli and relative permittivities $k_\mu = 10$ and $k_\varepsilon = 10$, respectively. The dash-dotted, continuous and dashed curves are for the volume fractions $c^{(i)} = 0.283$ (corresponds to the diameter $d = 0.6a$), 0.196 (corresponds to the diameter $d = 0.5a$) and 0.126 (corresponds to the diameter $d = 0.4a$), respectively. The arrows indicate the transition from the stable to unstable domains. Indeed, in the absence of an electric field the critical stretches correspond to the case of the purely mechanical loading. Fig. 4(a) shows the results for the case when the electric field is aligned with the stretch direction, while Fig. 4(b) corresponds to the case when the electric field is applied perpendicularly to the stretch direction. We observe that the critical stretch is a monotonically decreasing function of an electric field for the aligned case (Fig. 4(a)). When the electric field is applied perpendicularly to the stretch direction (Fig. 4(b)), the critical stretch increases with an increase in the electric field, thus, manifesting in a stabilizing effect of the electric field in this case. DE composites become more stable with a decrease in the volume fraction of the inclusion for both directions of the applied electric field. The dashed curve, corresponding to the DE with the lowest considered volume fraction $c^{(i)} = 0.196$ (corresponds to the diameter $d = 0.4a$), is above the solid and dash-dotted curves for all values of the applied electric field (see Fig. 4).

Note that in this work we prescribe the deformation together with the applied electric field, and identify the stable and unstable domains in terms of these two electromechanical loading parameters. Alternatively, one can specify electric field and applied tractions $\mathbf{t} = \boldsymbol{\sigma}\mathbf{n}$ (where $\mathbf{n}$ is the outward normal), and find a loading path for these conditions in terms of calculated deformations or actuations. The reported in Fig. 4 curves separate the stable and unstable domains for a variety of applied combinations of electric field and tractions. To illustrate this we plot in Fig. 5 the dependence of the stretch on the applied electric field for the DE composites subjected to different constant tractions. The dimensionless traction is normalized by the shear modulus of the matrix, namely $\tilde{\mathbf{t}} = \mathbf{t}/\mu^{(m)}$. The dashed, dotted and dash-dotted curves correspond to the tractions $\tilde{t}_2 = -3.8$, $\tilde{t}_2 = -3.7$ and $\tilde{t}_2 = -3.5$, respectively. We observe that stretch increases with an increase in the electric field. A decrease in the absolute value of traction shifts the curve to the left side. The continuous curve in Fig. 5 corresponds to the onset of instability for the composite (which is also shown by the dashed curve in Fig. 4(b)). The shaded region above the continuous curve represents the unstable domain. The intersection points of the continuous and dashed ($\hat{E}_2^0 = 0.15, \overline{\lambda}_c = 1.77$), continuous and dotted ($\hat{E}_2^0 = 0.25, \overline{\lambda}_c = 1.78$), and continuous and dash-dotted

[1] This is based on our numerical observations and analytical predictions for effective permittivity of the 2D unit cell, where the circular inclusion is assumed to be significantly stiffer than the matrix phase (for example, $k_\mu = 50, 100$); thus, one can obtain an explicit expression for effective permittivity as functions of stretch based on the results by Sihvola and Lindell, 1992, Kärkkäinen et al., 2000.

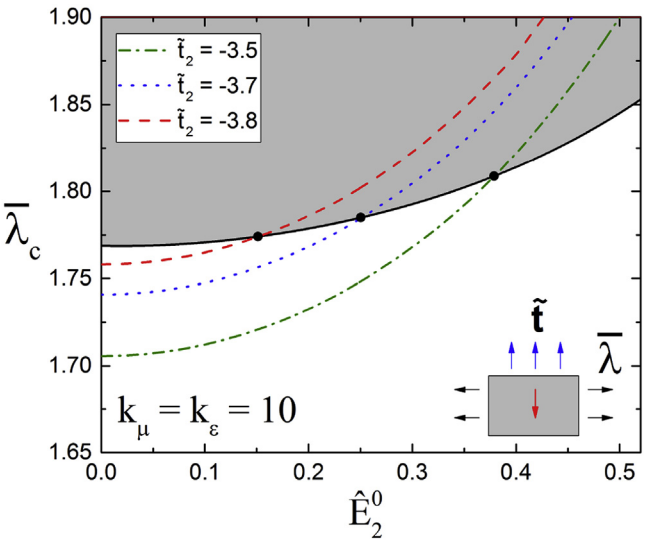

Fig. 5. Stretch vs electric field for the DE composite subjected to different constant tractions. The contrast in the shear moduli and relative permittivities is $k_\mu = k_\varepsilon = 10$. The volume fraction of the inclusion is $c^{(i)} = 0.126$ (corresponds to the diameter $d = 0.4a$). The continuous curve corresponds separates the stable and unstable (grey area) domains.

$(\hat{E}_2^0 = 0.38, \bar{\lambda}_c = 1.81)$ curves correspond to the onset of the electromechanical instabilities along the corresponding loading paths with different tractions. The continuous curve represents the set of onset of instability points for all possible applied tractions.

Next, we present the dependence of the critical stretch on the contrast in the shear moduli k_μ. The contrast in the relative permittivities of the phases is kept fixed at the value $k_\varepsilon = 10$. The dash-dotted, continuous and dashed curves correspond to the electric fields $\tilde{E}_1^0 = 1$, $\tilde{E}_1^0 = 0.5$ and $\tilde{E}^0 = 0$ in Fig. 6(a), and $\tilde{E}_2^0 = 0.2$, $\tilde{E}_2^0 = 0.1$ and $\tilde{E}^0 = 0$ in Fig. 6(b), respectively. We observe that the critical stretch decreases with an increase in the contrast in the shear moduli. We find that, for any contrast in the shear moduli, the electric field aligned with the stretch direction ($\mathbf{e}_1$-axis) promotes instabilities (see Fig. 6(a)), whereas the electric field applied perpendicularly to the stretch direction stabilizes the DE composites (see Fig. 6(b)). We also observe a rapid increase in the critical stretch as the contrast in the shear moduli decreases towards the mechanically homogeneous composites ($k_\mu = 1$). The corresponding curves flatten with a further increase in the shear moduli $k_\mu \gtrsim 60$.

The dependence of the critical stretch on the contrast in both shear moduli and electric permittivities is shown in Fig. 7. The dash-dotted, continuous and dashed curves correspond to the electric fields $\tilde{E}_2^0 = 0.4$, $\tilde{E}_1^0 = 1$ and $\tilde{E}^0 = 0$, respectively. The volume fraction of the inclusion is $c^{(i)} = 0.283$ (corresponds to the diameter $d = 0.6a$). We observe that an increase in the phase contrast leads to a decrease in the critical stretch. Consistently with the previous observations, we find that the critical stretch dashed-dotted curve for the case when the electric field applied perpendicularly to the stretch direction, appears above the dashed curve corresponding to the purely mechanical loading ($\bar{E} = 0$), and also above the curve corresponding to the case when the electric field is aligned with the stretch direction in Fig. 7.

Next, we examine the influence of the relative permittivity ratio k_ε on the critical stretch for composites with the fixed contrast in the shear moduli $k_\mu = 10$. The dependence of the critical stretch on the contrast in relative permittivities is shown in Fig. 8(a). The dash-dotted, continuous and dashed curves correspond to the response of DE composites subjected to the electric fields $\tilde{E}_2^0 = 0.4$, $\tilde{E}_1^0 = 1$ and $\tilde{E}^0 = 0$, respectively. The volume fraction of the inclusion phase is $c^{(i)} = 0.283$ (corresponds to the diameter $d = 0.6a$). The electric field stabilizes composite when applied perpendicularly to the stretch direction, and the electric field promotes instabilities when applied in the stretch direction ($\mathbf{e}_1$). However, we observe that the curves $\bar{\lambda}_c(k_\varepsilon)$ flatten for both directions of the applied electric field with an increase in relative permittivity ratio. To provide more details on this behavior we plot the dependence of the average electric field in the matrix and inclusion phases on the relative permittivity ratio in Fig. 8(b). The results are presented for the applied electric field is $\tilde{E}_2^0 = 0.4$ and stretch $\bar{\lambda} = 1.1$. The dotted horizontal line corresponds to the average electric field $\tilde{E}_2 = \bar{\lambda}\,\tilde{E}_2^0 = 0.44$ in the deformed state. The dash-dotted and continuous curves correspond to the current electric fields in the matrix and inclusion phases, respectively. We observe that for a high relative permittivity $\varepsilon^{(i)}$, the electric field almost does not penetrate into the inclusion phase. When $\varepsilon^{(i)}$

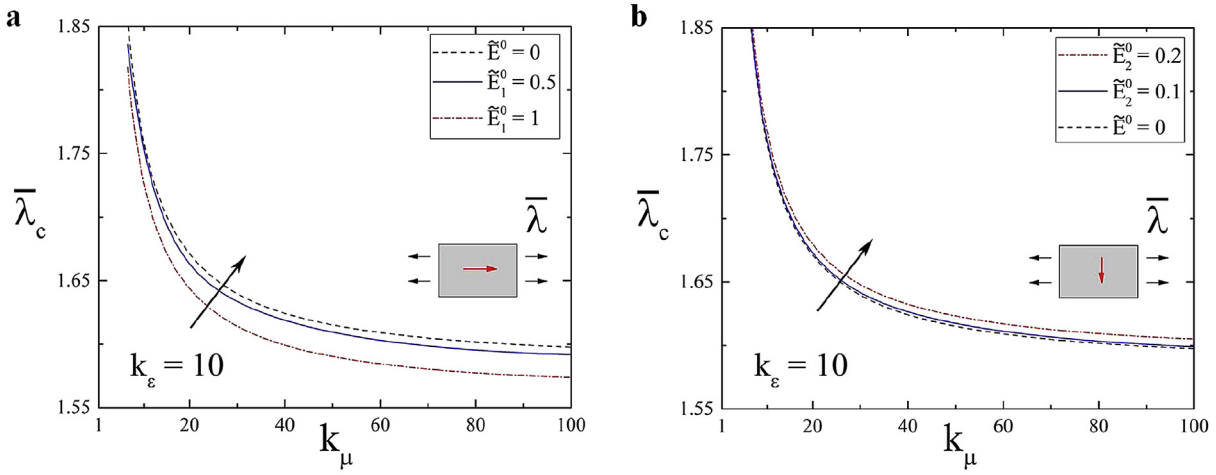

Fig. 6. Critical stretch vs contrast in the shear moduli for composites with the contrast in relative permittivities $k_\varepsilon = 10$. (a) - the electric field is aligned with the stretch direction, (b) - the electric field applied perpendicularly to the stretch direction. The volume fraction of the inclusion phase is $c^{(i)} = 0.126$ (corresponds to the diameter $d = 0.4a$).

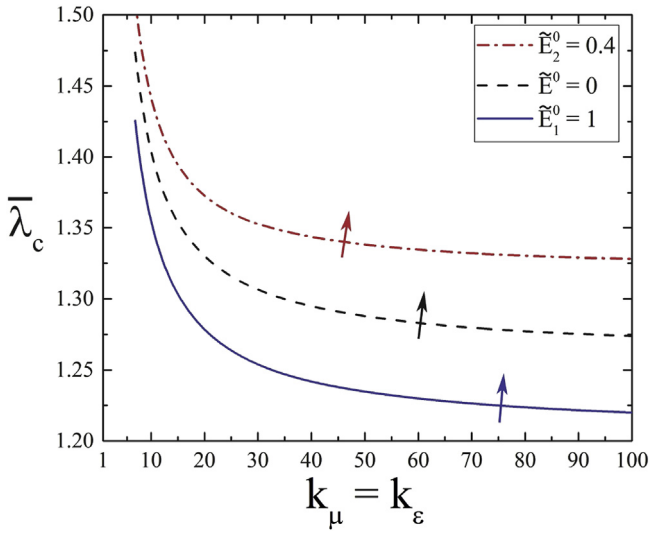

Fig. 7. Critical stretch vs phase material property contrast. The volume fraction of the inclusion is $c^{(i)} = 0.283$ (corresponds to the diameter $d = 0.6a$).

approaches infinity, the electric field and the associated electrostatic stresses in the inclusion phase vanish while the corresponding electrostatic part of the total stresses in the matrix phase reach a saturation value. Consequently, the influence of the contrast in the phase permittivities on the critical stretch ratio reduces, so the corresponding curves (see the dash-dotted and continuous curves in Fig. 8(a)) asymptotically approach a constant value. We note that for permittivity ratio $\varepsilon_2/\varepsilon_1 = 1$ we obtain the same critical stretch regardless the direction and magnitude of the applied electric field; in such case, the stability is fully determined by the mechanical properties of the phases.

To illustrate the influence of phase volume fractions on the onset of the electromechanical instability, we plot the critical stretch as a function of inclusion volume fraction in Fig. 9. The dash-dotted, continuous and dashed curves correspond to the electric fields $\tilde{E}_2^0 = 0.3$, $\tilde{E}_1^0 = 0.6$ and $\tilde{E}^0 = 0$, respectively. The contrasts in the shear moduli and relative permittivities are $k_\mu = k_\varepsilon = 10$ in Fig. 9(a) and $k_\mu = k_\varepsilon = 50$ in Fig. 9(b). In a manner similar to the purely mechanical case, we observe that the critical stretch decreases with an increase in the inclusion volume fraction. This decrease is greater at lower volume fractions $c^{(i)} \lesssim 0.2$ than at

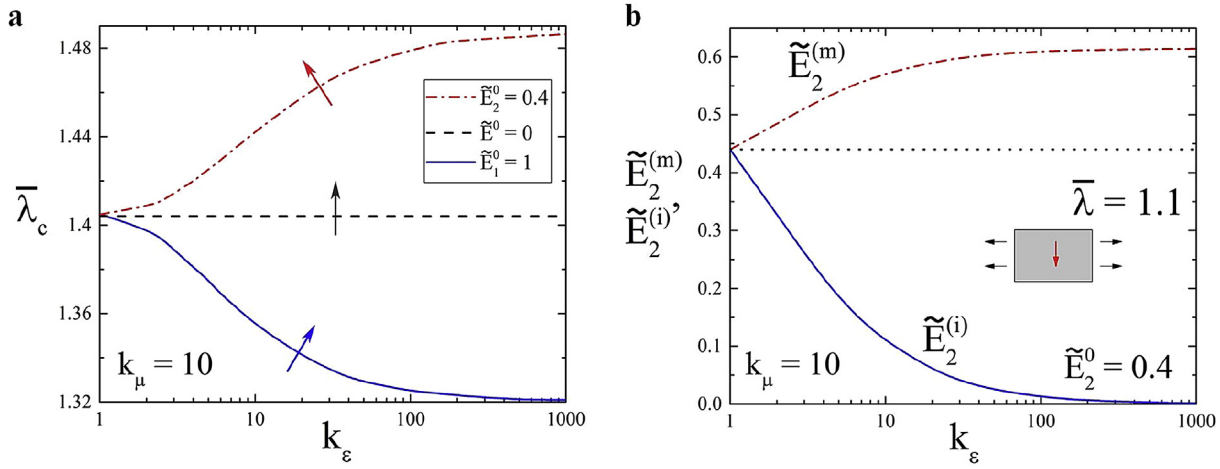

Fig. 8. (a) - critical stretch vs relative permittivity ratio, (b) - the dependence of the average electric field in the matrix and inclusion phases for DE composites with the contrast in the shear moduli $k_\mu = 10$. The volume fraction of the inclusion phase is $c^{(i)} = 0.283$ (corresponds to the diameter d = 0.6a).

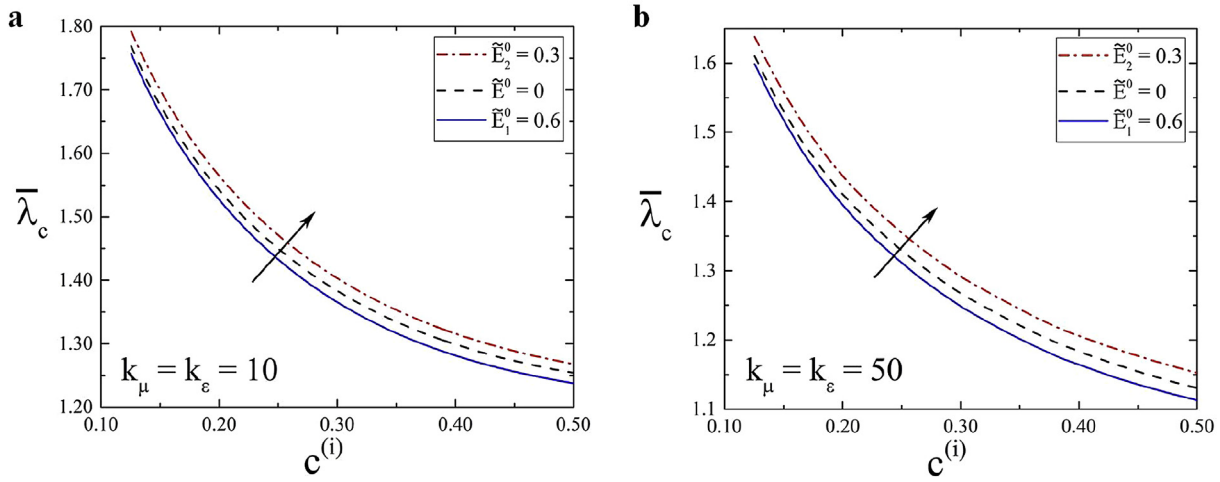

Fig. 9. Critical stretch vs volume fraction of the inclusion phase for DE composites with the contrasts in shear moduli and relative permittivities $k_\mu = k_\varepsilon = 10$ (a) and $k_\mu = k_\varepsilon = 50$ (b).

moderate ones $c^{(i)} \gtrsim 0.4$. Similar to the previous observations, we find that the electric field stabilizes the composite if applied perpendicularly to the stretch direction, while the electric field applied in the stretch direction promotes instabilities.

4.2. DE composites with periodically arranged elliptical inclusions

Next we investigate the behavior of periodic DE composites with elliptical inclusions embedded in a soft matrix. The schematic illustration of the periodic composites and corresponding unit cell are shown in Fig. 2(b) and (c). The ratio between the length of the sides of the rectangular unit cell is $a/b = 1.5$. The volume fraction of the inclusion is defined by $c^{(i)} = \pi r_1 r_2/(ab)$. In the non-aligned case, when the inclination angle of the elliptical inclusion in the undeformed configuration is $\alpha \neq 0, \pi/2$, the particle rotates with the applied tension. As a result, more complicated distributions of the stress and electric field components is induced by a macroscopically applied electromechanical loading, as compared to the aligned case ($\alpha = 0, \pi/2$). An example of the inhomogeneous distributions of the deviatoric parts of the Cauchy stress components and electric field are shown in Fig. 10. The DE composite with the volume fraction of the inclusion $c^{(i)} = 0.136$ is subjected to the stretch $\overline{\lambda} = 1.55$. The aspect ratio and inclusion inclination angle are $w = r_1/r_2 = 2$ ($r_2 = 0.18a$) and the inclusion inclination angle is $\alpha = \pi/4$. The contrast ratios are $k_\mu = k_\varepsilon = 50$ ($\mu^{(m)} = 1$ MPa and $\varepsilon^{(m)} = 5$). The field distributions are presented for the applied electric fields $\widehat{E}_1^0 = 1$ in Fig. 10(a), (c), (e) and (d), and for $\widehat{E}_2^0 = 0.3$ in Fig. 10(b), (d), (f) and (h). We note that the applied electromechanical loading ($\widehat{E}_1^0 = 1$, $\overline{\lambda} = 1.55$) corresponds to the onset of the electromechanical instabilities. We observe that the highest stresses appear in the regions near the inclusion for both directions of the applied electric field (see Fig. 10(a)-(d)). Note that relatively high concentrations of the electric fields are found at the regions near the inclusion. This is despite the fact that the corresponding average values of these fields equal to zero, $\overline{E}_1 = 0$ in Fig. 10(f), and $\overline{E}_2 = 0$ in Fig. 10(g). However, the electric field almost does not penetrate the inclusion. In Fig. 10(e) and (h) we observe that the electric field in the inclusion is homogeneous and its absolute magnitude within the inclusion is smaller than the absolute value of the electric field in the matrix.

Finally, we investigate the stability of the DE composites with the periodically arranged elliptical inclusions. To illustrate the influence of the applied electromechanical loading on the stability of the DE composites, we plot the dependence of the critical stretch on the electric field for different inclination angles and aspect ratios of the elliptical inclusion in Fig. 11. The contrasts in shear moduli and relative permittivities are $k_\mu = 50$ and $k_\varepsilon = 10$, respectively. The volume fraction of the inclusion is kept constant at the value $c^{(i)} = 0.136$ (corresponds to $r_1 r_2 = 0.0648a^2$). The aspect ratio is

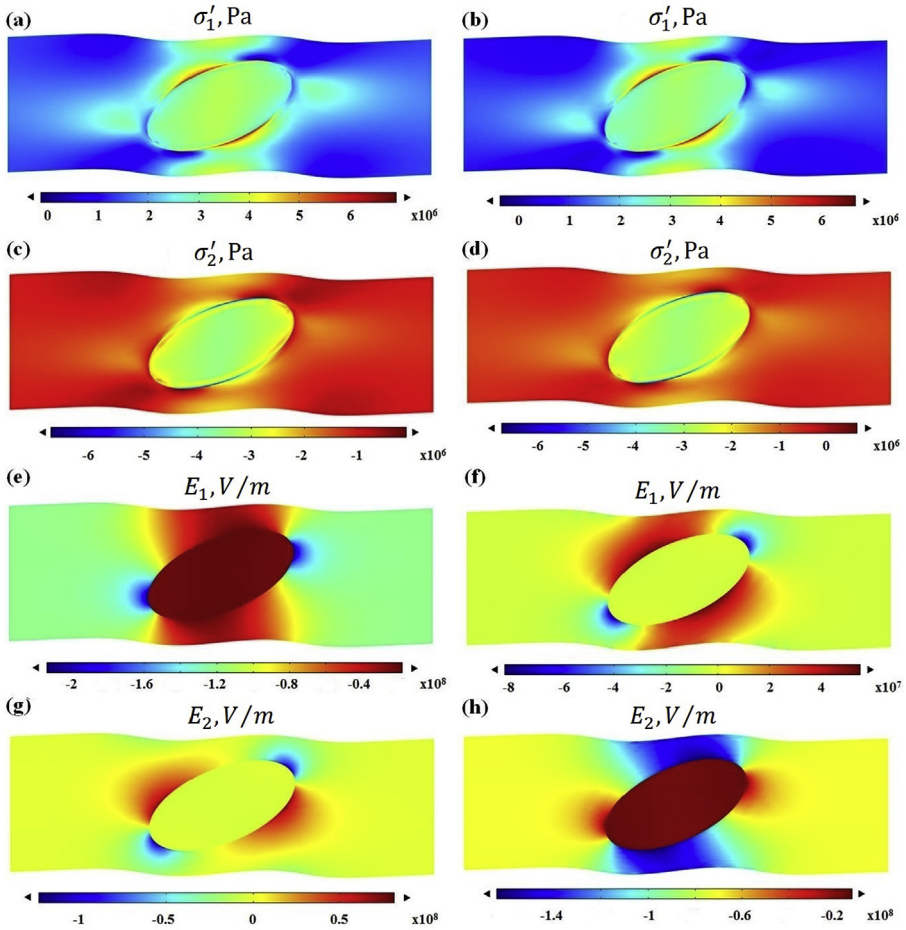

Fig. 10. Distribution of the deviatoric Cauchy stress components (a–d) and electric field (e–h) in the deformed unit cell under electric fields $\widehat{E}_1^0 = 1$ ((a),(c),(e),(g)), and $\widehat{E}_2^0 = 0.3$ ((b),(d),(f),(h)). The contrasts in the shear moduli and relative permittivities are $k_\mu = k_\varepsilon = 50$; $\mu^{(m)} = 1$ MPa and $\varepsilon^{(m)} = 5$. The volume fraction of inclusion phase and ellipticity aspect ratio of the particles are $c^{(i)} = 0.136$ and $w = 2$ (corresponds to the semi-major axis $r_1 = 0.36a$).

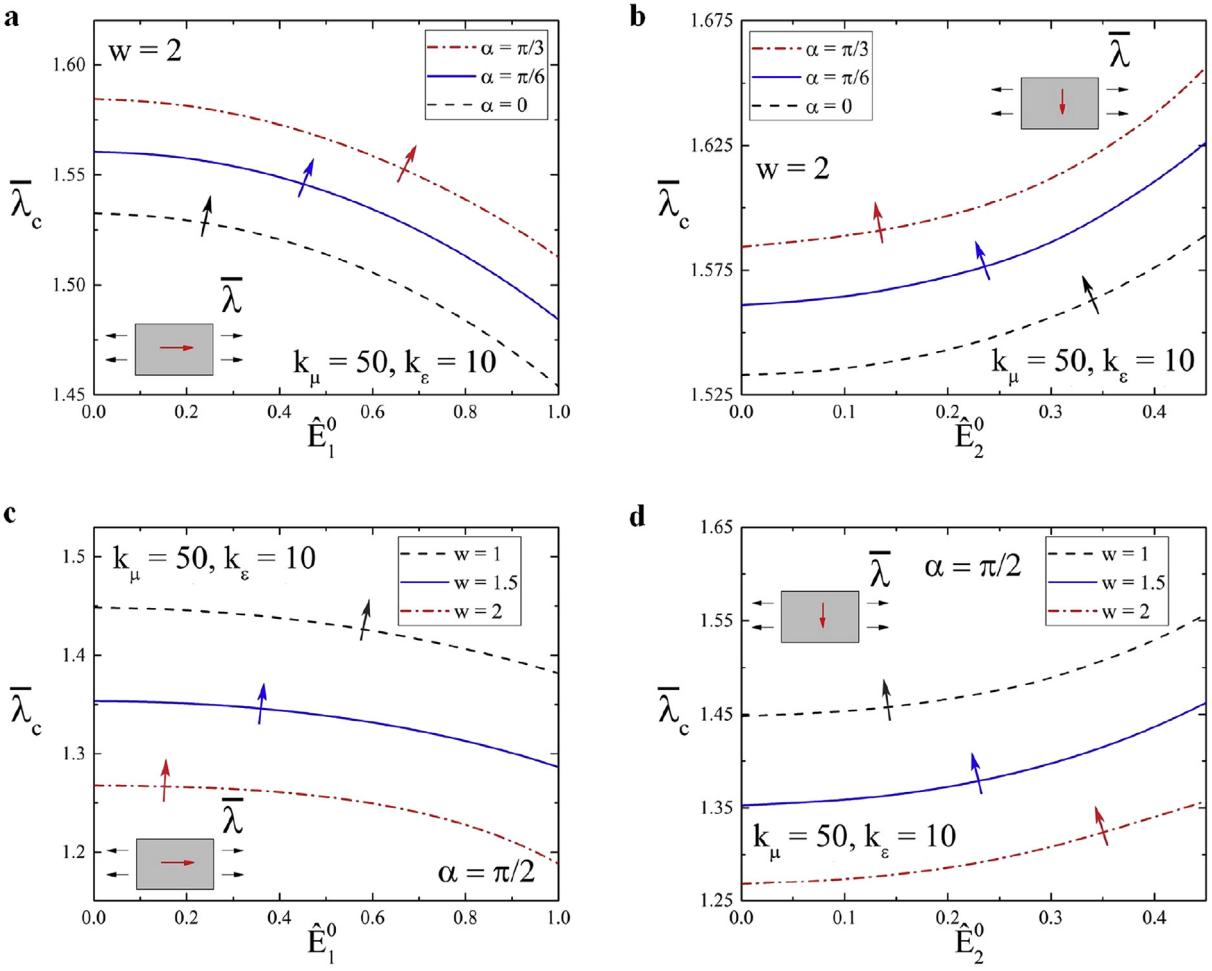

Fig. 11. Critical stretch ratio vs electric field for DE composites with the contrasts in shear moduli and relative permittivities $k_\mu = 50$ and $k_\varepsilon = 10$, respectively. (a) and (c) - the electric field is aligned with the stretch direction, (b) and (d) - the electric field is applied perpendicularly to the stretch direction. The aspect ratio is $w = 2$ in (a) and (b). The inclination angle is $\alpha = \pi/2$ in (c) and (d). The volume fraction of the inclusion is $c^{(i)} = 0.136$ (corresponds to $r_1 r_2 = 0.0648a^2$).

$w = 2$ in Fig. 11(a) and (b), and the inclination angle is $\alpha = \pi/2$ in Fig. 11(c) and (d). Similar to the observed behavior of the DE composites with circular inclusions (see Sec. 4.1), here we find that the electric field stabilizes the composite if applied perpendicularly to the stretch direction, and the electric field aligned with the stretch direction promotes instabilities. At the beginning, the critical stretch increases with an increase in the inclination angle. The dash-dotted curve (corresponding to $\alpha = \pi/3$) is above the continuous (corresponding to $\alpha = \pi/6$) and dashed (corresponding to $\alpha = 0$) curves for all values of the applied electric field (see Fig. 11(a) and (b)). However, a further increase in the inclination angle leads to a rapid decrease in the critical stretch. We find that the critical stretches for the DE composite with $\alpha = \pi/2$ (dash-dotted curves in Fig. 11(c) and (d)) are significantly smaller than for the DE composites with $\alpha = 0$ (dashed curves in Fig. 11(a) and (b)). The critical stretch decreases with an increase in the aspect ratio. The dash-dotted ($w = 2$) curve is below the solid ($w = 1.5$) and dashed curves ($w = 1$) for all values of the applied electric field (see Fig. 11(c) and (d)).

The dependence of the critical stretch on the inclusion inclination angle is shown in Fig. 12. The results are presented for DE composites with the volume fraction of inclusion $c^{(i)} = 0.136$ (corresponds to $r_1 r_2 = 0.0648a^2$), and with the contrasts in the shear moduli and relative permittivities are $k_\mu = 50$ and $k_\varepsilon = 10$, respectively. The dash-dotted, continuous and dashed curves correspond to the electric fields $\tilde{E}_2^0 = 0.3$, $\tilde{E}_1^0 = 1$ and $\tilde{E}^0 = 0$, respectively. The aspect ratio is $w = r_1/r_2 = 1.5$ in Fig. 12(a) and $w = 2$ in Fig. 12(b). For these non-aligned cases, we also observe that the electric field stabilizes the composite if applied perpendicularly to the stretch direction, and the electric field aligned with the stretch direction promotes instabilities. We observe a slight increase in the critical stretch before a point α_{max} where the curve $\overline{\lambda}_c(\alpha)$ reaches a maximum. This increase is followed by a relatively fast decrease in the critical stretch with a further increase in the inclination angle. The critical stretch reaches a minimum at $\alpha = \pi/2$ corresponding the most unstable configuration. The value of the inclination angle, associated with the maximum stretch, changes significantly with the change in the inclusion aspect ratio ($\alpha_{max} \approx 0.19\pi$ for $w = 1.5$ and $\alpha_{max} \approx 0.3\pi$ for $w = 2$). However, the value of the corresponding angle barely changes with a change in the electric field. An increase in the aspect ratio leads to a more pronounced dependence of the critical stretch on the inclination angle. For example, $(\overline{\lambda}_c)_{max} - (\overline{\lambda}_c)_{min} \approx 0.16$ for $w = 1.5$, and $(\overline{\lambda}_c)_{max} - (\overline{\lambda}_c)_{min} \approx 0.3$ for $w = 2$.

The dependence of the critical stretch on the aspect ratio of the elliptical particles is shown in Fig. 13. The examples are presented for DE composites with the contrasts in the shear moduli and

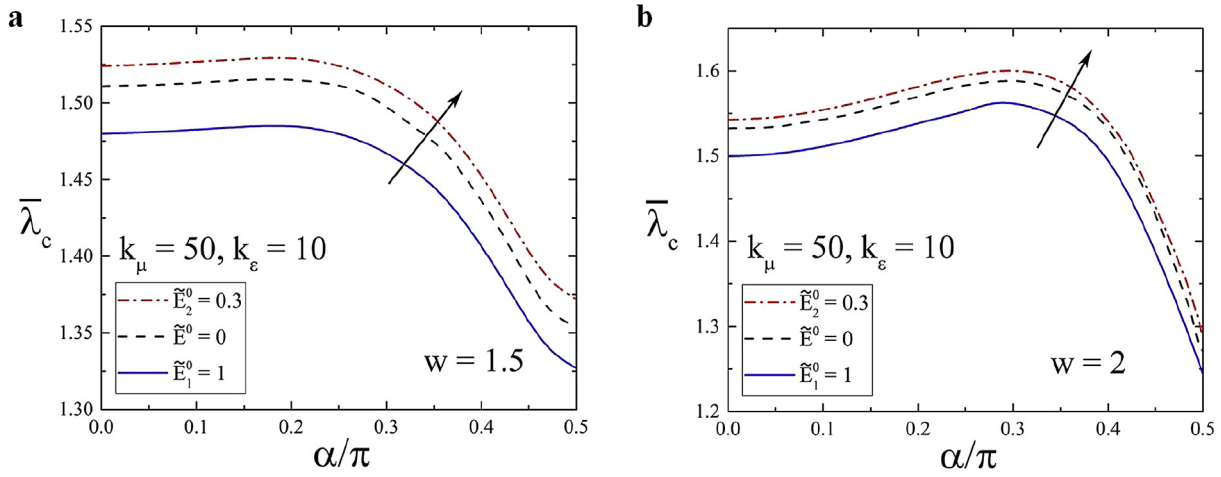

Fig. 12. Critical stretch vs inclination angle of the elliptical inclusion. The contrasts in the shear moduli and relative permittivities are $k_\mu = 50$ and $k_\varepsilon = 10$, respectively. The aspect ratios are $w = 1.5$ (a) and $w = 2$ (b). The volume fraction of the inclusion is $c^{(i)} = 0.136$ (corresponds to $r_1 r_2 = 0.0648a^2$).

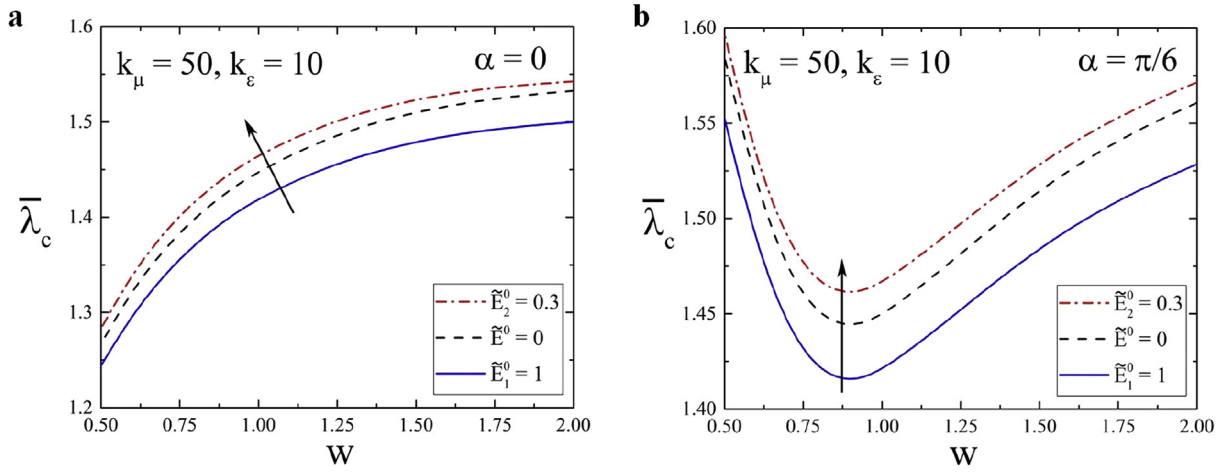

Fig. 13. Critical stretch vs aspect ratio of the elliptical inclusion for DE composites with the contrasts in the shear moduli and relative permittivities $k_\mu = 50$ and $k_\varepsilon = 10$, respectively. The inclination angles of the elliptical inclusions are $\alpha = 0$ (a) and $\alpha = \pi/6$ (b). The volume fraction of inclusion phase is $c^{(i)} = 0.136$ (corresponds to $r_1 r_2 = 0.0648a^2$).

relative permittivities $k_\mu = 50$ and $k_\varepsilon = 10$, respectively. The volume fraction is kept constant at the value $c^{(i)} = 0.136$ (corresponds to $r_1 r_2 = 0.0648a^2$). The dash-dotted, continuous and dashed curves are for the electric fields $\tilde{E}_2^0 = 0.3, \tilde{E}_1^0 = 1$ and $\tilde{E}^0 = 0$. The inclination angles are $\alpha = 0$ in Fig. 13(a) and $\alpha = \pi/6$ in Fig. 13(b). Consistently with the previous observations, we find that the electric field stabilizes the composite if applied perpendicularly to the stretch direction, and the electric field aligned with the stretch direction promotes instabilities. We observe that for the aligned case the critical stretch monotonically increases with an increase in aspect ratio w (see Fig. 13(a)). However, the behavior changes dramatically, when a non-aligned case ($\alpha = \pi/6$) is examined (see Fig. 13(b)). The critical stretch decreases fast and reaches a minimum for the aspect ratio $w_{min} \approx 0.9$, and, then, the critical stretch increases with a further increase in aspect ratio. The electric field almost does not influence the position of the most unstable configuration corresponding to w_{min}.

5. Conclusions

In this work, we examined the stability of periodic DE composites subjected to finite strains in the presence of an electric field. We implemented the stability analysis into a numerical finite element based tool, and through the numerical evaluation of the tensors of electroelastic moduli, the unstable domains were identified for periodic DE composites with circular and with elliptical inclusions embedded in a matrix. We studied the influence of the electromechanical loading (large deformations and electric field externally applied), and the geometrical and material parameters on the stability of the DE composites with particulate microstructures. We found that an electric field destabilized the composites when it was applied parallel to the stretch direction, and an electric field stabilized the composites when it was applied perpendicularly to the stretch direction. For periodic DE composites with circular inclusions, critical stretch was found to decrease with an increase in the volume fraction of the inclusion phase. An increase in the shear moduli contrast was found to promote instabilities in the DE composites. We observed that the role of the electric field became more significant with an increase in the dielectric constant contrast of the phases. For the DE composites with elliptical inclusions, we found that the inclusion inclination angle influenced the stability of the DE composites. In particular, the critical stretch curve was found to possess a unique maximum at a certain inclination angle.

The corresponding inclination angle is defined by the aspect ratio of the elliptical inclusion. When the elliptical inclusion was aligned with the stretch direction (the semi-major axis coincided with the stretch direction), we observed that an increase in the ellipticity aspect ratio resulted in a more stable behavior of the DE composites. In addition, we observed some deformation induced tunability of the components of the effective relative dielectric permittivity tensor in the periodic DE composites.

The analysis of the electromechanical instabilities takes into account the microstructure characteristics, which affect the effective electroelastic moduli, and, hence, the stability of the DE composites. However, microscopic instabilities may develop at the microstructure length-scales. To analyze the microscopic instabilities, a more involved analysis is required such as Bloch-Floquet type of analysis including the Bloch-Floquet conditions imposed on both mechanical and electric field variations; as opposite to the standard microscopic instability analysis for purely mechanical problems. The coupled microscopic instability analysis requires development of a new numerical tool, which can be developed in the future to predict the onset of instabilities at fine length scales.

These findings can be useful in further design of DE composites with enhanced properties and switchable functionalities. In addition, the presented analysis of the electromechanical instabilities can be applied to more complicated and richer multiphase periodic composites.

Acknowledgments

This research was supported by the Israel Science Foundation (grant 1550/15 and 19713/15). SR gratefully acknowledges the support of Taub Foundation through the Horev Fellowship – Leaders in Science and Technology.

References

Aboudi, J., 2015. Micro-electromechanics of soft dielectric matrix composites. Int. J. Solids Struct. 64, 30–41.
Bar-Cohen, Y., 2001. EAP history, current status, and infrastructure. In: Bar-Cohen, Y. (Ed.), Electroactive Polymer (EAP) Actuators as Artificial Muscles. SPIE press, Bellingham, WA, pp. 3–44. Ch. 1.
Bertoldi, K., Boyce, M.C., 2008. Wave propagation and instabilities in monolithic and periodically structured elastomeric materials undergoing large deformations. Phys. Rev. B 78, 184107.
Bertoldi, K., Gei, M., 2011. Instabilities in multilayered soft dielectrics. J. Mech. Phys. Solids 59, 18–42.
Bertoldi, K., Boyce, M.C., Deschanel, S., Prange, S., Mullin, T., 2008. Mechanics of deformation-triggered pattern transformations and superelastic behavior in periodic elastomeric structures. J. Mech. Phys. Solids 56 (8), 2642–2668.
Bortot, E., Denzer, R., Menzel, A., Gei, M., 2016. Analysis of viscoelastic soft dielectric elastomer generators operating in an electrical circuit. Int. J. Solids Struct. 78–79, 205–215.
Carpi, F., Frediani, G., Turco, S., De Rossi, D., 2011. Bioinspired tunable lens with muscle-like electroactive elastomers. Adv. Funct. Mater 21 (21), 4152–4158.
Cohen, N., deBotton, G., 2016. Electromechanical interplay in deformable dielectric elastomer networks. Phys. Rev. Lett. 116 (20), 208303.
Cohen, N., Dayal, K., deBotton, G., 2016. Electroelasticity of polymer networks. J. Mech. Phys. Solids 92, 105–126.
Dorfmann, A., Ogden, R.W., 2005. Nonlinear electroelasticity. Acta. Mech. 174, 167–183.
Dorfmann, A., Ogden, R.W., 2010. Nonlinear electroelastostatics: incremental equations and stability. Int. J. Eng. Sci. 48, 1–14.
Dorfmann, L., Ogden, R., 2014. Instabilities of an electroelastic plate. Int. J. Eng. Sci. 77, 79–101.
Ecer, A., 1973. Finite element analysis of the postbuckling structures behavior. AIAA J. 11 (11), 1532–1538.
Galich, P., Rudykh, S., 2016. Manipulating pressure and shear elastic waves in dielectric elastomers via external electric stimuli. Int. J. Solids Struct. 91, 18–25.
Galipeau, E., Rudykh, S., deBotton, G., Ponte Castañeda, P., 2014. Magnetoactive elastomers with periodic and random microstructures. Int. J. Solids Struct. 51, 3012–3024.
Gei, M., Roccabianca, S., Bacca, M., 2011. Controlling bandgap in electroactive polymer-based structures. Mechatronics, IEEE/ASME Trans. 16 (1), 102–107.
Hangai, Y., Kawamata, S., 1972. Perturbation Method in the Analysis of Geometrically Nonlinear and Stability Problems. Advances in Computational Methods in Structural Mechanics and Design. UAH Press, Huntsville, pp. 473–489.
Hill, R., 1972. On constitutive macro-variables for heterogeneous solids at finite strain. Proc. R. Soc. Lond. A 326, 131–147.
Huang, C., Zhang, Q.M., 2004. Enhanced dielectric and electromechanical responses in high dielectric constant all-polymer percolative composites. Adv. Funct. Mater 14, 501–506.
Itskov, M., Khiêm, V.N., 2014. A polyconvex anisotropic free energy function for electro-and magneto-rheological elastomers. Math. Mech. Solids 21 (9), 1126–1137.
Jabareen, M., 2015. On the modeling of electromechanical coupling in electroactive polymers using the mixed finite element formulation. Procedia IUTAM 12, 105–115.
Javili, A., Chatzigeorgiou, G., Steinmann, P., 2013. Computational homogenization in magneto-mechanics. Int. J. Solids Struct. 50 (25–26), 4197–4216.
Kärkkäinen, K.K., Sihvola, A.H., Nikoskinen, K.I., 2000. Effective permittivity of mixtures: numerical validation by the fdtd method. Geoscience Remote Sens. IEEE Trans. 38 (3), 1303–1308.
Keip, M., Steinmann, P., Schröder, J., 2014. Two-scale computational homogenization of electro-elasticity at finite strains. Comput. Methods Appl. Mech. Eng. 278, 62–79.
Keplinger, C., Li, T., Baumgartner, R., Suo, Z., Bauer, S., 2012. Harnessing snap-through instability in soft dielectrics to achieve giant voltage-triggered deformation. Soft Matter 8 (2), 285–288.
Kolle, M., Lethbridge, A., Kreysing, M., Baumberg, J., Aizenberg, J., Vukusic, P., 2013. Bio-inspired band-gap tunable elastic optical multilayer fibers. Adv. Mater 25 (15), 2239–2245.
Kornbluh, R.D., Pelrine, R., Prahlad, H., Wong-Foy, A., McCoy, B., Kim, S., Eckerle, J., Low, T., 2012. From boots to buoys: promises and challenges of dielectric elastomer energy harvesting. In: Electroactivity in Polymeric Materials. Springer, pp. 67–93.
Krishnan, D., Johnson, H., 2009. Optical properties of two-dimensional polymer photonic crystals after deformation-induced pattern transformations. J. Mech. Phys. Solids 57 (9), 1500–1513.
Lee, H., Fang, N., 2012. Micro 3d printing using a digital projector and its application in the study of soft materials mechanics. J. Vis. Exp. 69, e4457.
Li, T., Keplinger, C., Baumgartner, R., Bauer, S., Yang, W., Suo, Z., 2013. Giant voltage-induced deformation in dielectric elastomers near the verge of snap-through instability. J. Mech. Phys. Solids 61 (2), 611–628.
Li, X., Liu, L., Sharma, P., 2016. A new type of Maxwell stress in soft materials due to quantum mechanical-elasticity coupling. J. Mech. Phys. Solids 87, 115–129.
Liu, L., 2013. On energy formulations of electrostatics for continuum media. J. Mech. Phys. Solids 61 (4), 968–990.
McKay, T., O'Brien, B., Calius, E., Anderson, I., 2010. An integrated, self-priming dielectric elastomer generator. Appl. Phys. Lett. 97, 062911.
McMeeking, R.M., Landis, C.M., 2005. Electrostatic forces and stored energy for deformable dielectric materials. J. Appl. Mech. Trans. ASME 72, 581–590.
Ogden, R.W., 1974. On the overall moduli of non-linear elastic composite materials. J. Mech. Phys. Solids 22, 541–553.
Ogden, R.W., 2008. Nonlinear elasticity and fibrous structure in arterial wall mechanics. In: Lecture Notes for Summer School on Modeling and Computation in Biomechanics. Graz University of Technology, Austria.
Ortigosa, R., Gil, A.J., 2016. A new framework for large strain electromechanics based on convex multi-variable strain energies: conservation laws and hyperbolicity and extension to electro-magnetomechanics. Comput. Methods Appl. Mech. Engrg. 309, 202–242.
Pelrine, R.E., Kornbluh, R.D., Joseph, J.P., 1998. Electrostriction of polymer dielectrics with compliant electrodes as a mean of actuation. Sensors Actuators A 64, 77–85.
Pelrine, R., Kornbluh, R., Joseph, J., Heydt, R., Pei, Q.-B., Chiba, A., 2000a. High-field deformation of elastomeric dielectrics for actuators. Mater. Sci. Eng. 11, 89–100.
Pelrine, R., Kornbluh, R., Pei, Q.-B., Joseph, J., 2000b. High-speed electrically actuated elastomers with strain greater than 100%. Science 287, 836–839.
Plante, J.-S., Dubowsky, S., 2006. Large-scale failure modes of dielectric elastomer actuators. Int. J. Solids Struct. 43, 7727–7751.
Riks, E., 1984. Some computational aspects of the stability analysis of nonlinear structures. Comput. Methods Appl. Mech. Eng. 47 (3), 219–259.
Rudykh, S., Bertoldi, K., 2013. Stability of anisotropic magnetorheological elastomers in finite deformations: a micromechanical approach. J. Mech. Phys. Solids 61, 949–967.
Rudykh, S., Boyce, M., 2014. Transforming wave propagation in layered media via instability-induced interfacial wrinkling. Phys. Rev. Lett. 112, 034301.
Rudykh, S., deBotton, G., 2011. Stability of anisotropic electroactive polymers with application to layered media. Z. Angew. Math. Phys. 62, 1131–1142.
Rudykh, S., Bhattacharya, K., deBotton, G., 2012. Snap-through actuation of thick-wall electroactive balloons. Int. J. Nonlinear Mech. 47, 206–209.
Rudykh, S., Lewinstein, A., Uner, G., deBotton, G., 2013. Analysis of microstructural induced enhancement of electromechanical coupling in soft dielectrics. Appl. Phys. Lett. 102, 151905.
Rudykh, S., Bhattacharya, K., deBotton, G., 2014. Multiscale instabilities in soft heterogeneous dielectrics. Proc. R. Soc. A 470, 20130618.
Sihvola, A., Lindell, I., 1992. Polarizability modeling of heterogeneous media. In: Priou, A. (Ed.), Progress in Electromagnetics Research (PIER 6), Dielectric Properties of Heterogeneous Materials. Elsevier, Amsterdam, pp. 101–151. Ch. 3.

Singamaneni, S., Bertoldi, K., Chang, S., Jang, J.-H., Thomas, E.L., Boyce, M.C., Tsukruk, V.V., 2008. Instabilities and pattern transformation in periodic, porous elastoplastic solid coatings. ACS Appl. Mater. interfaces 1 (1), 42–47.
Singamaneni, S., Bertoldi, K., Chang, S., Jang, J., Young, S.L., Thomas, E.L., Boyce, M.C., Tsukruk, V.V., 2009. Bifurcated mechanical behavior of deformed periodic porous solids. Adv. Funct. Mater 19 (9), 1426–1436.
Slesarenko, V., Rudykh, S., 2016. Harnessing viscoelasticity and instabilities for tuning wavy patterns in soft layered composites. Soft Matter 12, 3677–3682.
Stoyanov, H., Kollosche, M., Risse, S., McCarthy, D., Kofod, G., 2011. Elastic block copolymer nanocomposites with controlled interfacial interactions for artificial muscles with direct voltage control. Soft Matter 7 (1), 194–202.
Suo, Z., Zhao, X., Greene, W.H., 2008. A nonlinear field theory of deformable dielectrics. J. Mech. Phys. Solids 56 (2), 467–486.
Tian, L., Tevet-Deree, L., deBotton, G., Bhattacharya, K., 2012. Dielectric elastomer composites. J. Mech. Phys. Solids 60, 181–198.
Toupin, R.A., 1956. The elastic dielectric. Arch. Ration. Mech. Anal. 5, 849–915.
Toupin, R.A., 1960. Stress tensors in elastic dielectrics. Arch. Ration. Mech. Anal. 5, 440–452.
Volokh, K., 2012. On electromechanical coupling in elastomers. J. Appl. Mech. 79 (4), 044507.
Vu, D.K., Steinmann, P., 2007. Nonlinear electro- and magneto-elastostatics: material and spatial settings. Int. J. Solids Struct. 44 (24), 7891–7905.
Wang, Q., Zhang, L., Zhao, X., 2011. Creasing to cratering instability in polymers under ultrahigh electric fields. Phys. Rev. Lett. 106 (11), 118301.
Zhao, X., Suo, Z., 2007. Method to analyze electromechanical stability of dielectric elastomers. Appl. Phys. Lett. 91 (6), 061921.
Zhao, X., Suo, Z., 2010. Theory of dielectric elastomers capable of giant deformation of actuation. Phys. Rev. Lett. 104 (17).
Zheng, X., Lee, H., Weisgraber, T.H., Shusteff, M., Deotte, J.R., Duoss, E., Kuntz, J.D., Biener, M.M., Ge, Q., Jackson, J.A., Kucheyev, S.O., Fang, N.X., Spadaccini, C.M., 2014. Ultra-light, ultra-stiff mechanical metamaterials. Science 344, 1373.